C. R. Mecanique 342 (2014) 46–51

Contents lists available at ScienceDirect

Comptes Rendus Mecanique

www.sciencedirect.com

Toward glasses with better indentation cracking resistance

Tanguy Rouxel [a,*], Pathikumar Sellappan [b], Fabrice Célarié [a], Patrick Houizot [a], Jean-Christophe Sangleboeuf [a]

[a] Applied Mechanics Laboratory of the University of Rennes 1, LARMAUR, ERL CNRS 6274, Université de Rennes-1, campus de Beaulieu, 35042 Rennes cedex, France
[b] Department of Materials Science and Engineering, University of Illinois at Urbana–Champaign, IL, USA

ARTICLE INFO

Article history:
Received 6 September 2013
Accepted after revision 16 October 2013
Available online 4 December 2013

Keywords:
Glass
Mechanical behavior
Indentation
Deformation
Cracking

ABSTRACT

The microcracking sequence (radial, median, lateral, and ring-like) arising at the glass surface under sharp contact loading and the extent to which these cracks develop is intimately related to the way the material attempts to relax the corresponding stress field. Two processes which are known to occur upon indentation are densification and isochoric shear flow. The contributions of both mechanisms were quantitatively assessed for glasses belonging to different chemical systems in previous papers [1–3]. In the present study, indentation cracking maps are provided, which offer guidelines to the design of glasses with better surface damage resistance based on their elastic properties and hardness.

1. Introduction

A sharp contact loading at the surface of a glass leaves a permanent imprint mostly accompanied by various types of microcracks which form either on loading or on unloading, some of which extending radially from the indentation axis (radial cracks) or forming half-penny cracks beneath the indent in planes containing the load axis (median cracks), others showing up as concentric segments (ring or cone cracks) and some extending under the surface, and almost parallel to it, at least in the beginning of the process (lateral cracks). Although this problem has already motivated numerous studies the conclusions regarding the dependence on the composition remain limited so far to a rough classification between glasses preferentially exhibiting cone cracking (the so-called anomalous glasses) and those for which radial–median cracks predominate (the so-called normal glasses) [4–8].

Major obstacles to reach a better understanding of the incidence of the composition lie in the complexity and the diversity of the indentation cracking patterns (Fig. 1). It turns out that ring cracks tend to form in low Poisson's ratio (ν) glasses such as vitreous silica, whereas the most easily damaged glasses – i.e. those opposing the smallest resistance to indentation corner cracking – possess the largest ν values among oxide glasses. However, at ν values above 0.35, microcracking becomes limited and eventually disappears, as for Zr-based or precious metal-based metallic glasses [10,11].

2. Driving force for indentation cracking

The volume of matter displaced on indentation needs to be accommodated within the half-infinite material surrounding the indentation site. An analysis of this problem in the far field – i.e. far enough from the indentation process zone where different irreversible mechanisms (densification, shear flow, phase transformation) take place – can be limited to linear elasticity. By superposing the Boussinesq stress field [13] originating from a point-load normal to the surface of a semi-infinite

* Corresponding author.

1631-0721/$ – see front matter
http://dx.doi.org/10.1016/j.crme.2013.10.008

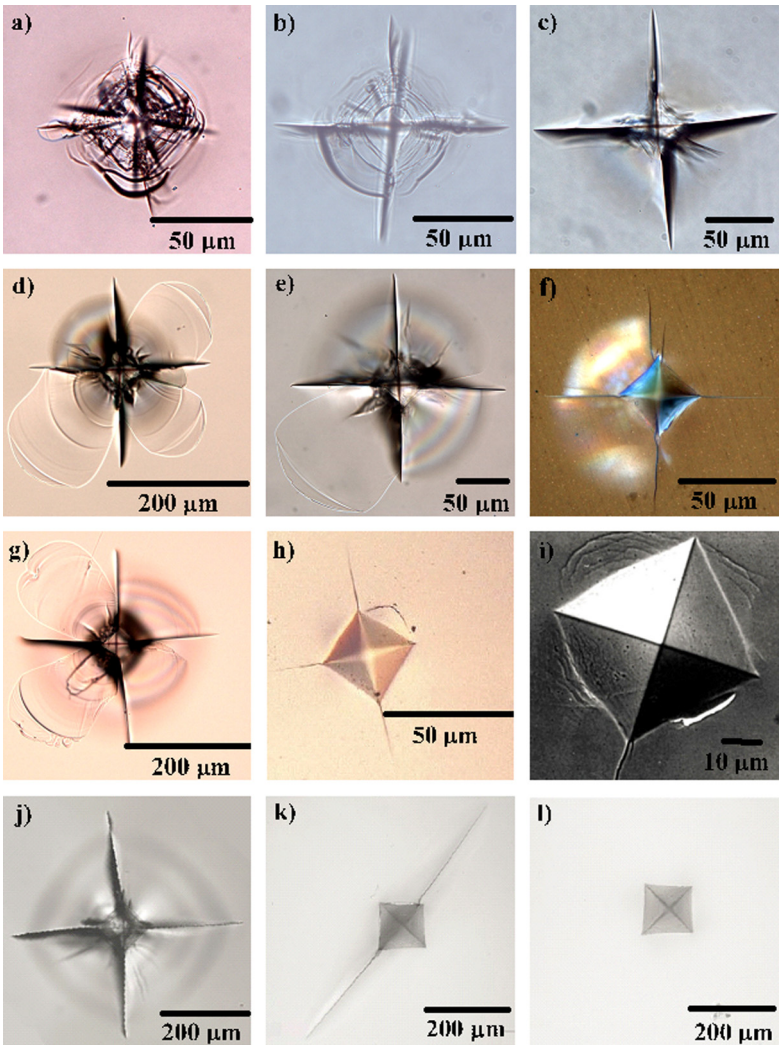

Fig. 1. (Color online.) Optical microscope observation of indentation cracking patterns produced by Vickers indentation: Indentation load of 9.81 N for 15 s for glasses with different Poisson's ratio (ν), Young's modulus (E) and hardness (H), from left to right: (a) a-SiO_2 (0.15, 8.7, 8.05), (b) borosilicate ($Si_{0.25}B_{0.08}Na_{0.03}O_{0.64}$) (0.195, 6.7, 10.05), (c) soda-lime silicate ($Si_{0.25}Na_{0.08}Mg_{0.01}Ca_{0.04}O_{0.61}$) (0.227, 6.3, 11.8), (d) lead silicate ($Si_{0.20}Pb_{0.2}Na_{0.01}O_{0.59}$) (0.253, 4.1, 13.3), (e) boro-alumino silicate ($Si_{0.13}B_{0.16}Al_{0.01}Na_{0.01}Ba_{0.08}O_{0.61}$) (0.264, 6.57, 13.3), (f) oxynitride silicate ($Ca_{12.26}Si_{10}O_{19}N_{8.84}$) [9] (0.291, 9.7, 11.7), (g) fluorite ($P_{0.04}F_{0.36}Al_{0.07}Li_{0.03}Mg_{0.02}Ca_{0.04}Sr_{0.05}Ba_{0.02}O_{0.37}$) (0.298, 4.5, 17.9), (h) iron-based bulk metallic glass ($Fe_{0.41}Co_{0.07}Cr_{0.15}Mo_{0.14}C_{0.15}B_{0.06}Y_{0.02}$) [10] (0.337, 13, 17.4), (i) palladium-based bulk metallic glass ($Pd_{0.4}Ni_{0.0}P_{0.2}$) [11] (0.4, 6, 18); (j) to (l): soda-lime-silica (planilux – Saint-Gobain) (0.234, 5.9, 12.5) for 49 N load at 20, 450 and 480 °C [12]. The stoichiometric compositions are limited to elements present at contents larger than 1 at.%. Numbers in brackets represent (ν, H (GPa), E/H).

elastic body (Young's modulus, E, and Poisson's ratio, ν) and a field stemming from a strain nucleus built on three double forces of the same intensity [14], Yoffe [15] proposed a field having the ability to remarkably well describe the various indentation cracking features. It comes that ring, radial, lateral, and median cracks are essentially driven by $\sigma_{rr}(\theta = \pi/2)$, $\sigma_{\phi\phi}(\theta = \pi/2)$, $\sigma_{rr}(\theta = 0)$ and $\sigma_{\theta\theta}(\theta = 0)$ respectively (spherical coordinates, with origin on the surface at contact point, θ the angle to the loading axis and ϕ the angle around this axis). Normalized to hardness (H), these components write:

$$\sigma_{rr}(r = a, \theta = \pi/2)/H = \frac{1-2\nu}{2} + \frac{2(\nu-2)\xi}{\pi(1+\nu)(1-2\nu)\tan\psi}(E/H) \tag{1}$$

$$\sigma_{\phi\phi}(r = a, \theta = \pi/2)/H = \frac{2\nu-1}{2} + \frac{2\xi}{\pi(1+\nu)\tan\psi}(E/H) \tag{2}$$

$$\sigma_{rr}(r = a, \theta = 0)/H = -\frac{3}{2}\frac{6\xi}{\pi(1+\nu)(1-2\nu)\tan\psi}(E/H) \tag{3}$$

$$\sigma_{\theta\theta}(r = a, \theta = 0)/H = \frac{1-2\nu}{4}\frac{\xi}{\pi(1+\nu)\tan\psi}(E/H) \tag{4}$$

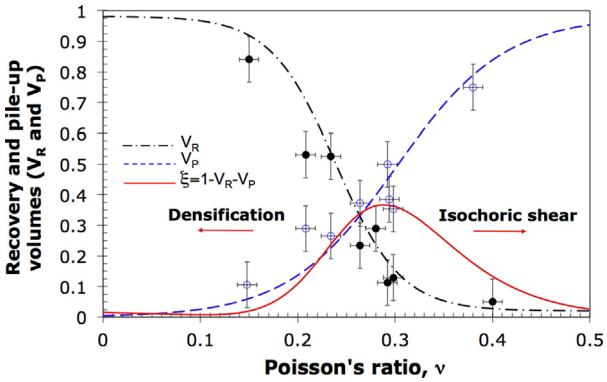

Fig. 2. (Color online.) Recovery (V_R) (solid marks) and pile-up (V_P) (empty marks) volume ratios (fitting of the data from Refs. [1–3,19]), as estimated by a topological analysis of the indentation site by means of AFM, as a function of Poisson's ratio.

where the first term on the right hand side comes from the Boussinesq stress field, and the second one (the so-called "blister" field) was proposed by Yoffe to take into account the residual stress field, ψ ($= 70.3°$) is the equivalent conical indenter which would produce a circular imprint (radius R) of the same projected area as for the Vickers indent (diagonal $2a$), so that $\pi R^2 = 2a^2$, and ξ is a tunable parameter between 0 and 1 governing the intensity of the residual stress field.

These expressions, set for the loading stage, were taken at $r = a$ and normalized to hardness for convenience. The stress field arising on loading is load independent due to the geometrical similarity of the problem. Nevertheless, the situation is different during the unloading stage since the blister field strength remains unchanged (due to the irreversible densification and to the permanent pile-up of matter) while the Boussinesq field, purely elastic, decreases linearly with P, so that microcracking might occur on unloading in some cases as the sign of a stress component changes from negative to positive. Surprisingly, so far most of the studies dealing with the sharp-contact loading problem [8,15] were conducted assuming a given value for ν (mostly 0.25, as proposed by Poisson himself whatever the material) although a glance at the governing equations (Eqs. (1) to (4)) shows that ν is obviously playing a key role. Remark that it is even the sole material characteristics involved in the Boussinesq stress field [13]. Besides, it was shown in a previous study [3] that the parameter ξ which is of paramount incidence strongly depends on ν and can be estimated quantitatively. Nevertheless, the magnitude of the blister field when neither densification nor shear flow come into play ($\xi = 0$) as well as the concomitant incidence of microcracking on the resulting stress field deserve further investigations.

3. Stress relaxation processes

Two mechanisms account for the reduction – or the relaxation – of the residual stress field, namely densification and isochoric shear flow [2]. Indentation involves stresses large enough to promote the densification of matter – both in the area of contact and in a region typically $\sim 1/3$ of the indentation size depth. This is because the disordered atomic structure of glass allows a significant amount of free volume, especially in glasses with a large fraction of glass-forming elements, such as silica-rich silicate glasses. Indeed the instantaneous elastic response of the material to the sharp contact loading induces a contact stress as high as $E/[2(1-\nu)\tan\psi]$ [14,16], i.e. typically over 10 GPa for silicate glasses. The contribution of the densification process depends much on the glass composition and can be as high as 84% of the residual indentation volume in a-SiO_2 and is less than 5% in the case of bulk metallic glasses [1,17,18] (Fig. 2). For a window glass, it is typically close to 60%. The indentation behavior was investigated at constant loading rate on mirror polished surfaces with a dwell time at maximum load of 15 s using a diamond Vickers indenter for a load from 10 mN to 10 N. All measurements were performed in a thermally regulated room, at 20 °C in air. All characteristics were averaged over measurements on 8 indentations per grade. Hardness values were calculated using the average indentation diagonal length as estimated using optical and scanning electron microscopes. Hardness was calculated using $H = \frac{P}{2a^2}$, where P (in Newton) is the peak load applied on the indenter and a (in meter) is half of the diagonal length. The fractions of the indentation volume (permanent imprint) attributed to densification and shear, namely V_R and V_P (associated with the pile-up of matter in the vicinity of the indent) respectively, were quantitatively estimated using Atomic Force Microscopy. The details of the experimental procedure are given in Refs. [1,3]. Then, in Eqs. (1)–(4), $\xi = 1 - V_R - V_P$.

It has long been considered that vitreous silica (a-SiO_2) is the unique candidate for indentation–densification. This is likely another reason why so little attention was paid to ν in the mechanical analysis of the indentation problem, although ν was recently found to reflect the extent to which densification contributes in glasses from different chemical systems [20]. Indeed, a remarkable correlation was found between ν and the atomic packing density of the glass network [21]. As expected, V_R monotonically decreases as ν increases (Fig. 2). On the contrary, V_P increases with ν and this can be viewed as an evidence for more shear ductility at large ν combined with a decrease of the densification contribution. It is noteworthy that the extent of pile-up also scales with the packing density in granular systems [22]. ξ is found to exhibit a maximum of 0.38 at $\nu \sim 0.29$. It is observed that while glasses with $\nu < 0.2$ are submitted to relatively small residual stresses (especially

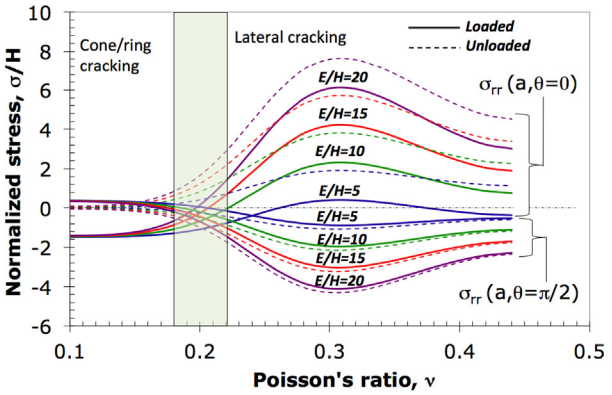

Fig. 3. (Color online.) Driving force for ring/cone cracking ($\sigma_r(r=a,\theta=\pi/2)$) and subsurface lateral cracking ($\sigma_r(r=a,\theta=0)$) for different E/H ratios as a function of ν. Curves are drawn from Eqs. (1) and (3).

tensile components), a dramatic increase of the driving force for lateral cracking ($\sigma_{rr}(\theta=0)$) is expected as ν increases above 0.2 (Fig. 3).

Furthermore, whereas $\sigma_{rr}(\theta=\pi/2)$ and $\sigma_{\theta\theta}(\theta=0)$ are negative after complete unloading whatever ν, $\sigma_{rr}(\theta=0)$ and $\sigma_{\phi\phi}(\theta=\pi/2)$ become positive on unloading so that lateral and radial cracks might show up during the unloading stage. This behavior was indeed reported by means of in-situ observations in soda-lime-silica (SLS) and alumino-silicate glasses ($E/H\sim 11$–13, $\nu\sim 0.2$–0.21), which experience little – or no – cracking on loading thanks to the moderated intensity of the stress field in this $(E/H,\nu)$ range, while radial – and lateral – cracking occur on unloading [4,5,8]. Note in Fig. 3 that most oxide glasses lie in a rather small area bounded by $E/H\sim 10$–12 and $\nu\sim 0.2$–0.3. Metallic glasses mostly correspond to $E/H>14$ and $\nu>0.32$, that is in a range where the stress components tend to decrease with increasing ν. Large E/H ratios, typically above 15, are common for crystalline materials so that the radial cracks mostly occur early on loading. The E/H ratio is typically larger than a few hundreds for ductile metals, which are known to exhibit extensive pile-up of matter in the vicinity of the indent (isochoric shear flow), so that the occurrence of ring or median cracks is very unlikely, inasmuch ν is also large for ductile materials. The transition from ring ("anomalous" glasses) to radial as well as lateral cracking ("normal" glasses) extends from $\nu=0.18$ and $\nu=0.22$ depending on the E/H ratio. Note that whereas densification prevails at small ν values and represents over 50% of the indentation volume at $\nu<0.2$, isochoric shear flow (shear plasticity) is highly promoted and favors a ductile behavior in glasses with ν larger than 0.3 – for instance, silicon oxynitride and metallic glasses, corroborating the fact that the fracture energy of bulk metallic glasses with $\nu>0.32$ exceeds the one of oxide glasses by 2 to 4 orders of magnitude [23].

4. Indentation cracking map

Fig. 4 shows the boundaries of the different microcracking regimes in E/H versus ν maps. The predictions are mostly in good agreement with the experimental observations. For instance, in the case of vitreous silica $(\nu,E/H)=(0.15,8.05)$, ring cracks are predicted, in agreement with the observation in Fig. 1(a). The borosilicate glass lies almost on the boundary between compressive and tensile stresses for ring and median–radial cracking, so that both occur but remain limited (Fig. 1(b)). As a matter of fact, borosilicate glasses offer a remarkable resistance toward surface damage by indentation and scratching. Radial and lateral cracking is expected in the soda-lime-silica glass (Fig. 1(c)) and in a greater extent in the lead-silicate and in the boro-alumino silicate glasses (Figs. 1(d) and 1(e)). Eventually, in the latter case, lateral cracking develops to such an extent that chips form. The larger ν for the oxynitride glass [9] (Fig. 1(f)) is compensated by an E/H ratio smaller than for the boro-alumino silicate glass, so that the microcracking patterns of both glasses look very similar. The fluorite glass, combining a ν of 0.298 and an E/H ratio as large as 17.9, suffers from extensive indentation cracking (Fig. 1(g)). As ν becomes larger than 0.33, volume conservative shear flow relays on densification and promotes efficient stress relaxation. Thus, relatively small radial cracks are visible in the Fe-based metallic glass ($\nu=0.35$) [10] and even smaller (or none) for the Pd-based glass ($\nu=0.4$) [11]. In the latter case, note the presence of concentric shear bands in the vicinity of the indentation, which indicates the onset of a ductile behavior. As the temperature is raised to T_g, shear flow becomes easier and in the meantime ν increases while E/H decreases, so that a better resistance to microcracking follows (Figs. 1(k) and 1(l)). The intensity of the stress field is relatively moderated for E/H between 11 and 13 and ν close to 0.2, as evidenced on all maps in Fig. 4.

Hence microcracking is expected to be limited on loading in alumino-silicate and soda-lime-silicate glasses (in this range) consistently with in-situ observations [4–7,24]. It is noteworthy that the low brittleness silica-rich glass developed by Sehgal and Ito [25], with $E/H\sim 14.7$ and $\nu\sim 0.18$, lies precisely on the zero-stress contours in Figs. 4(b) and 4(d) and in the compressive stress regions in Figs. 4(a) and 4(c), so that the indentation cracking maps provide an explanation for the absence of cracks for such a glass composition. On the contrary, in several crystalline materials [8] such as sapphire ($E/H\sim 16$–17 and $\nu\sim 0.25$) and MgO ($E/H\sim 25$) and $\nu\sim 0.21$ radial cracks form almost immediately on loading, probably

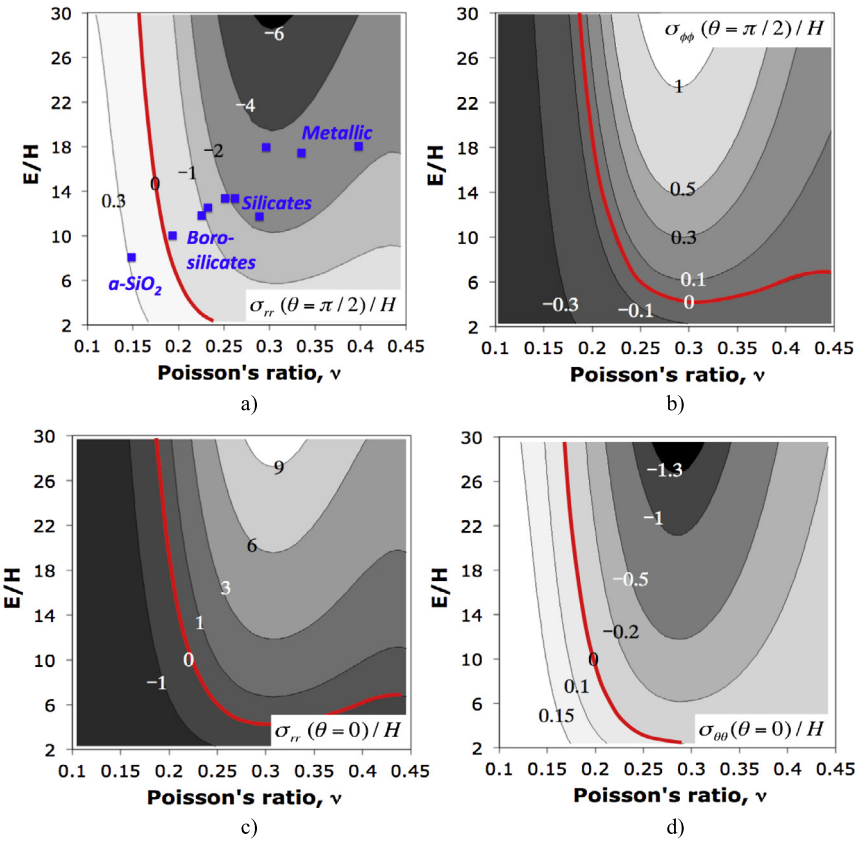

Fig. 4. (Color online.) Map of the stress field rising on loading at a Vickers indentation site as a function of ν and the E/H ratio. The stress field components were calculated using Eqs. (1)–(4) at a distance $r = a$ from the initial contact point at the surface and for $\theta = 0$ (along the vertical axis) and $\theta = \pi/2$ (surface), and normalized to hardness for convenience. The (thick) red contour indicates the region where the stress component vanishes. (a) $\delta_{rr}(r = a, \theta = \pi/2)/H$, governing the formation of ring cracks (the square marks correspond to the glasses considered in Fig. 1); (b) $\delta_{\phi\phi}(r = a, \theta = \pi/2)/H$, driving force for the radial cracks, (c) $\delta_{rr}(r = a, \theta = 0)/H$, driving force for the lateral cracks, and (d) $\delta_{\theta\theta}(r = a, \theta = 0)/H$, which is assumed to govern the formation of the median cracks.

because of relatively large E/H ratios for ν values comparable to those of glasses. A comparison between Figs. 4(b) and 4(c) shows that as E/H decreases for a fixed ν value, median cracks might take over radial ones as $\sigma_{\phi\phi}(\pi/2)$ becomes negative while $\sigma_{\theta\theta}(\theta = 0)$ becomes positive, in agreement with a numerical study by Lee et al. [26] who predicted the predominance of median cracks over radial-like surface cracks as Young's modulus is divided by two while ν remains constant (see Fig. 9 in Ref. [26]). The model is also corroborated by the temperature dependence of the indentation cracking behavior. On the one hand, as a glass is cooled down from the glass transition temperature, its hardness increases faster than its stiffness (in the case of a-SiO_2 a decrease of E is even observed on cooling) so that E/H decreases while a light decrease of ν is expected. For example, in the case of soda-lime-silica glass and fused silica at $-196\,^{\circ}$C, $(E/H, \nu)$ equals $(6.7, 0.23)$ and $(3, 0.14)$ respectively, so that radial–median cracking becomes less favorable, as was observed by Kurkjian et al. [24]. On the other hand, when T increases from 20 to 450 °C, the values of E/H and ν ratios of a standard window glass increase from ~ 10 to ~ 20 and from 0.235 to ~ 0.24, respectively, so that corner cracks become longer and better defined [12], as observed in Fig. 1(k). At higher temperature, the contribution of shear flow is large enough to suppress any visible microcracks (Fig. 1(l)). The present analysis also provides an explanation for the change from radial to ring cracking in crystalline materials subsequently to a raise of the vacancy concentration due to ion implantation, for instance [27]. This defect population is expected to give more room for the densification process and is likely to induce a decrease in ν, so that $\sigma_{\phi\phi}(\pi/2)$ will eventually become negative (Fig. 4(a)), while $\sigma_r(\pi/2)$ becomes positive (Fig. 4(b)). Nevertheless, the present analysis does not encompass all indentation cracking scenario and only provides some guidelines to reduce the residual stress field stemming from sharp contact loading. The way cracks alter the stress field as they develop and might interact with each other was eluded. Furthermore, one must keep in mind that whether cracks will form or not ultimately depends on fracture toughness, which is also a composition-dependent characteristic.

5. Conclusion

Indentation cracking maps were proposed to predict the microcracking pattern from E/H versus ν. A critical value for ν (~ 0.22) was brought to light, at which the intensity of the indentation stress field tends to vanish, preventing

crack formation on loading, while the driving force after unloading remains small. Four major groups of glasses can be differentiated in view of their resistance toward corner cracks (i.e. radial–median), namely: (i) *resilient* glasses, for $0.15 < \nu < 0.20$; (ii) *semi-resilient* glasses, for $0.20 < \nu < 0.25$; and (iii) *easily damaged* glasses for $0.25 < \nu < 0.33$, and (iv) *highly resilient* for $0.33 < \nu$.

Acknowledgements

The European Research Council is greatly acknowledged for the Advanced Grant 320506 (DAMREG) of the 7th framework program "Ideas". The authors are indebted to Prof. R. Conradt and to Dr. E. Becker (RWTH, Aachen, Germany), to Saint-Gobain Company, and to Arc International Inc. for supplying the oxide glass specimens. Dr. J.-P. Guin (LARMAUR, University Rennes-1) is greatly acknowledged for the AFM observations and analysis. One of the authors, Dr. P. Sellappan, is indebted to the French Ministry of Higher Education for PhD fellowship.

References

[1] S. Yoshida, et al., Quantitative evaluation of indentation-induced densification in glass, J. Mater. Res. 20 (2005) 3404–3412.
[2] T. Rouxel, et al., Indentation deformation mechanism in glass: Densification versus shear flow, J. Appl. Phys. 107 (2010) 094903.
[3] P. Sellappan, et al., Composition dependence of indentation deformation and indentation cracking in glass, Acta Mater. 61 (2013) 5949–5965.
[4] A. Arora, et al., Indentation deformation/fracture of normal and anomalous glasses, J. Non-Cryst. Solids 31 (1979) 415–428.
[5] A.G. Evans, T.R. Wilshaw, Quasi-static particle damage in brittle solids – I. Observations, analysis and implications, Acta Metall. 24 (1976) 939–956.
[6] B.R. Lawn, A.G. Evans, A model for crack initiation in elastic/plastic indentation fields, J. Mater. Sci. 12 (1977) 2195–2199.
[7] J.T. Hagan, M.V. Swain, The origin of median and lateral cracks around plastic indents in brittle materials, J. Phys. D: Appl. Phys. 11 (1978) 2091–2102.
[8] R.F. Cook, G.M. Pharr, Direct observation and analysis of indentation cracking in glasses and ceramics, J. Am. Ceram. Soc. 73 (1990) 787–817.
[9] P. Sellappan, et al., Elastic properties and surface damage resistance of nitrogen-rich (Ca, Sr)–Si–O–N glasses, J. Non-Cryst. Solids 356 (2010) 2120–2126.
[10] V. Keryvin, V.H. Hoang, J. Shen, On the deformation morphology of bulk metallic glasses underneath a Vickers indentation, Intermetallics 17 (2009) 211.
[11] U. Ramamurty, et al., Hardness and plastic deformation in a bulk metallic glass, Acta Mater. 53 (2005) 705–717.
[12] K. Kese, et al., Effect of high temperature ambience during sharp indentation on the residual contact site properties, J. Phys. D: Appl. Phys. 41 (2008) 074025.
[13] J. Boussinesq, Applications des potentiels à l'étude de l'équilibre et du mouvement des solides élastiques, Gauthier-Villars, Paris, 1885.
[14] A.E.H. Love, A Treatise on the Mathematical Theory of Elasticity, Dover Pub. Inc., 1927, p. 127.
[15] E.H. Yoffe, Elastic stress fields caused by indenting brittle materials, Philos. Mag. A 46 (1982) 617–628.
[16] I.N. Sneddon, The relation between load and penetration in the axi-symmetric Boussinesq problem for a punch of arbitrary profile, Int. J. Eng. Sci. 3 (1965) 47–57.
[17] S. Yoshida, et al., Shrinkage behavior of Knoop indentations in silica and soda-lime-silica glasses, J. Am. Ceram. Soc. 84 (2001) 2141–2143.
[18] J.E. Neely, J.D. Mackenzie, Hardness and low-temperature deformation of silica glass, J. Mater. Sci. 3 (1968) 603–609.
[19] Y. Kato, et al., Effect of densification on crack initiation under Vickers indentation test, J. Non-Cryst. Solids 356 (2010) 1768–1773.
[20] T. Rouxel, Poisson's ratio and the densification of glass under high pressure, Phys. Rev. Lett. 100 (2008) 225501.
[21] G.N. Greaves, et al., Poisson's ratio and modern materials, Nat. Mater. 10 (2011) 823–837.
[22] E. Hamm, F. Tapia, F. Melo, Dynamics of shear bands in a dense granular material forced by a slowly moving rigid body, Phys. Rev. E 84 (2011) 041304.
[23] S.V. Madge, et al., Toughness, extrinsic effects and Poisson's ratio of bulk metallic glasses, Acta Mater. 60 (2012) 4800–4809.
[24] C.R. Kurkjian, G.W. Kammlott, M.M. Chaudhri, Indentation behavior of soda-lime silica glass, fused silica, and single-crystal quartz at liquid nitrogen temperature, J. Am. Ceram. Soc. 78 (1995) 737–744.
[25] J. Sehgal, S. Ito, A new low-brittleness glass in the soda-lime-silica glass family, J. Am. Ceram. Soc. 81 (1998) 2485–2488.
[26] J.H. Lee, et al., Cohesive interface simulations of indentation cracking as a fracture toughness measurement method for brittle materials, Acta Mater. 60 (2012) 5448–5467.
[27] D.J. Oliver, et al., Nanoindentation of ion-implanted crystalline germanium, Phys. Rev. B 80 (2009) 115210.